BIOCHEMISTRY
including biophysical chemistry & molecular biology

Article

pubs.acs.org/biochemistry

Structural Basis of the Substrate Specificity of Cytidine Deaminase Superfamily Guanine Deaminase

Aruna Bitra, Anwesha Biswas, and Ruchi Anand*

Department of Chemistry, Indian Institute of Technology, Mumbai 400076, India

Supporting Information

ABSTRACT: Guanine deaminases (GDs) are important enzymes involved in purine metabolism as well as nucleotide anabolism pathways that exhibit a high degree of fidelity. Here, the structural basis of the substrate specificity of GDs was investigated by determining a series of X-ray structures of NE0047 (GD from *Nitrosomonas europaea*) with nucleobase analogues and nucleosides. The structures demonstrated that the interactions in the GD active site are tailor-made to accommodate only guanine and any substitutions in the purine ring or introduction of a pyrimidine ring results in rearrangement of the bases in a catalytically unfavorable orientation, away from the proton shuttling residue E143. In addition, X-ray structural studies performed on cytidine revealed that although it binds in an optimal conformation, its deamination does not occur because of the inability of the enzyme to orchestrate the closure of the catalytically important C-terminal loop (residues 181−189). Isothermal calorimetry measurements established that these nucleoside moieties also disrupt the sequential mode of ligand binding, thereby abrogating all intersubunit communication. Intriguingly, it was recently discovered that GDs can also serve as endogenous ammeline deaminases, although it is structurally nonhomologous with guanine. To understand the mechanism of dual-substrate specificity, the structure of NE0047 in complex with ammeline was determined to a resolution of 2.7 Å. The structure revealed that ammeline not only fits in the active site in a catalytically favorable orientation but also allows for closure of the C-terminal loop.

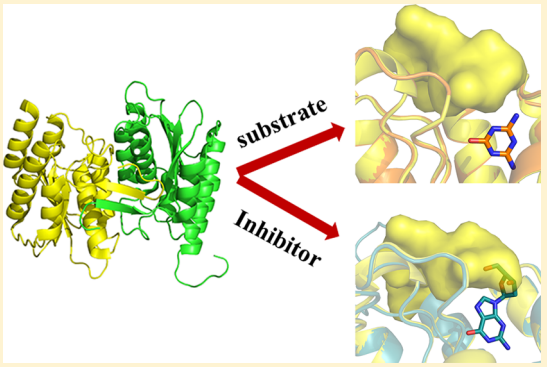

Guanine deaminases (GDs) are important enzymes in prokaryotic and eukaryotic systems.[1−4] Under conditions where the usual nitrogen sources obtained via the glutamine and ammonia processing pathways are unavailable, purines are used as the sole nitrogen source by many organisms.[5] Deamination of guanine serves as the first committed step in purine metabolism and is responsible for the removal of guanine from the total guanylic pool via hydrolytic degradation to xanthine and ammonia in a metal-assisted fashion[2,5,6] (Scheme 1A). In 2010, it was established by Wackett and co-workers that GDs also catalyze the deamination of triazine-based compound ammeline to ammelide (Scheme 1B). Ammeline is an intermediate in the melamine pathway, which is responsible for conversion of melamine to cyanuric acid.[7] It was demonstrated that while there were specific enzymes for other reactions in the melamine degradation pathway, eukaryotic GDs are the sole endogenous enzymes that were responsible for the deamination of ammeline.[8] Melamine is a chemical adulterant in pet food and infant formula, which has been attributed to melamine poisoning in pets;[9] more than 1000 deaths have been attributed to acute kidney disease.[10]

There are two major classes of GDs reported in the literature; many eukaryotic, fungal, and bacterial species like *Escherichia coli* possess the triosephosphate isomerase (TIM) amidohydrolase (AHS) superfamily GDs.[11−13] Other organisms like plants, archaea, and some species such as *Bacillus subtilis* harbor GDs that belong to the cytidine deaminase (CDA) superfamily.[2,14,15] Both classes of GDs are evolutionarily distinct and exhibit almost no apparent similarity in their folds. However, both the GDs utilize metals as cofactors, which not only are essential for maintaining the structural integrity of the fold but also play a pivotal role in deamination. *B. subtilis* GD (bGD) was the first GD belonging to the CDA superfamily that was structurally characterized (PDB entry 1WKQ). The X-ray structure showed that it exists as a domain-swapped functional dimer exhibiting an $\alpha\beta\alpha$ layer fold consisting of five central β-strands, which are flanked by helices on either side.[2,6] Recently, the X-ray structure of another GD belonging to the CDA superfamily, NE0047, was determined (PDB entries 2G84 and 4HRQ), and it was revealed that unlike bGD, it does not exhibit domain swapping.[16] Moreover, it was established that NE0047, like the eukaryotic AHS GD, can act as an ammeline deaminase, although with a slightly reduced catalytic efficiency (10^5 M^{-1} s^{-1} for guanine vs 10^3 M^{-1} s^{-1} for ammeline). The mechanism of deamination in CDA GDs was also investigated, and it was shown that there are two crucial negatively charged amino acids that act as proton shuttles, facilitating deamination.[16,17] In the case of GD from *Nitrosomonas europaea*, E79 activates the catalytic water molecule

Received: June 24, 2013
Revised: October 1, 2013
Published: October 1, 2013

   dx.doi.org/10.1021/bi400818e | *Biochemistry* 2013, 52, 8106−8114

Scheme 1. Reactions Catalyzed by Guanine Deaminase from *Nitrosomonas europaea* (NE0047)

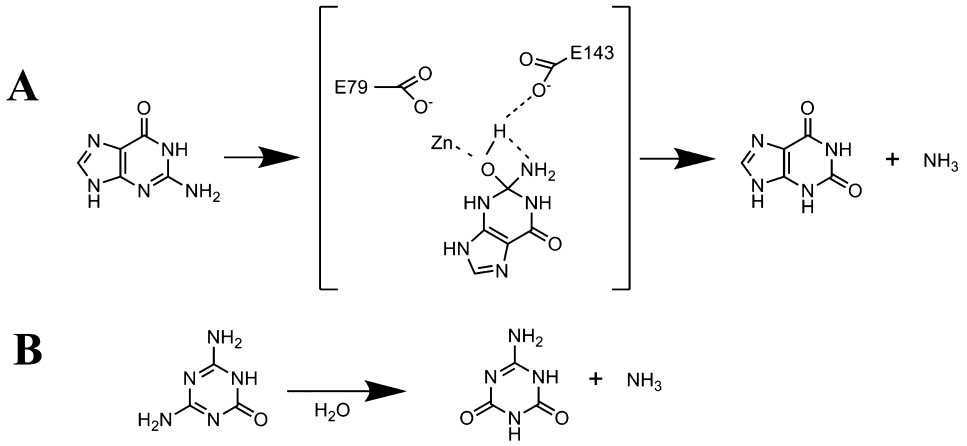

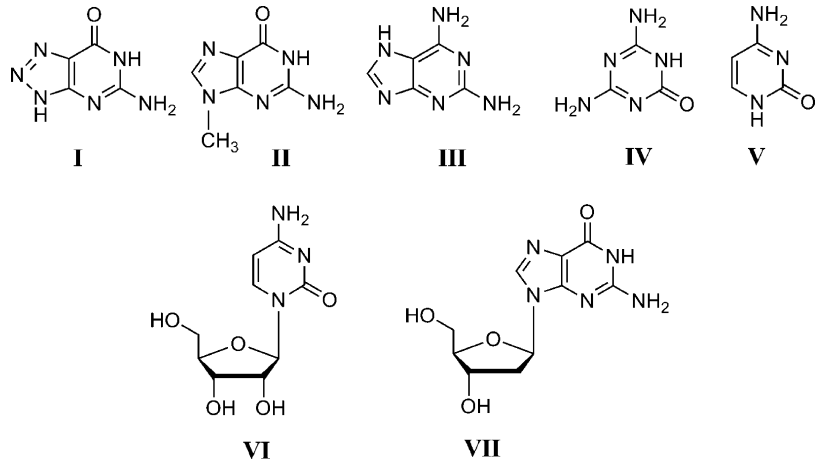

Figure 1. Compounds used for structural characterization: (I) 8-azaguanine, (II) 9-methylguanine, (III) 2,6-diaminopurine, (IV) ammeline, (V) cytosine, (VI) cytidine, and (VII) 2′-deoxyguanosine.

that is coordinated to the zinc atom and the generated hydroxide nucleophile attacks the C2 atom adjacent to the amino group, resulting in the formation of a tetrahedral intermediate. The collapse of this intermediate and subsequent release of ammonia are assisted by E143 (Scheme 1A).[16] In addition, the importance of the C-terminal loop in the CDA GDs was also emphasized, and it was shown that the extreme C-terminus of the protein played a crucial role in the progress of the reaction by protecting the reaction intermediate from the solvent.[16]

Previously, activity assay measurements on NE0047 have shown that GDs belonging to the CDA family are very sensitive to perturbation of the guanine scaffold.[16] Alternate nucleobases, their analogues, or their respective nucleosides and nucleotides are not accepted as substrates by this enzyme.[16] In this study, to understand the structural basis of substrate specificity, we determined the X-ray structures of NE0047 in complex with various guanine analogues and with representative nucleosides whose structures are depicted in Figure 1. In addition, because GDs accept the structurally nonhomologous six-membered heterocyclic compound ammeline, the dual-substrate specificity exhibited by GDs was investigated by performing X-ray crystallographic and ITC studies. Moreover, the question of why GDs are unable to catalyze alternate six-membered heterocyclic compounds other than ammeline (such as cytosine) was also addressed.

MATERIALS AND METHODS

Protein Expression and Purification of NE0047. The NE0047 plasmid was a gift from the Midwest structural genomics consortium group in Toronto, Canada. All the mutants of NE0047 were made by site-directed mutagenesis using the Kapa Hifi polymerase enzyme. Full length native NE0047 (residues 1−195) and an extremely C-terminally deleted construct (residues 1−180) were expressed as six-His tag fusion proteins. All the procedures for protein expression and purification were the same as those described previously.[16] The activity assay for determining the liberation of ammonia by NE0047 and its variants was performed using the Berthelot reaction.[18]

Crystallization, Data Collection, and Refinement. A total of six structures are reported: (a) NE0047−9-methylguanine complex (PDB entry 4LC5), (2) NE0047−2,6-diaminopurine complex (PDB entry 4LCP), (3) NE0047−cytidine complex (PDB entry 4LD2), (4) NE0047−2′-deoxyguanosine complex (PDB entry 4LCN), (5) NE0047−ammeline complex (PDB entry 4LCO), and (6) NE0047−cytosine complex (PDB entry 4LD4). The chemical structures of all these ligands are shown in Figure 1. Crystallization of all these complexes was performed by the hanging drop vapor diffusion method at 18 °C. Except cytidine and 2′-deoxyguanosine, the remaining ligands are insoluble in water; therefore, these ligands were solubilized by the addition of

dx.doi.org/10.1021/bi400818e | *Biochemistry* 2013, 52, 8106−8114

Table 1. Data Processing and Refinement Statistics

	NE0047−9-methylguanine (PDB entry 4LC5)	NE0047−2,6-diaminopurine (PDB entry 4LCP)	NE0047−cytidine (PDB entry 4LD2)	NE0047−2′-deoxyguanosine (PDB entry 4LCN)	NE0047−ammeline (PDB entry 4LCO)	NE0047−cytosine (PDB entry 4LD4)
			Data Collection[a]			
resolution (Å)	2.00	2.0	1.55	1.8	2.7	3.0
space group	$P2_12_12_1$	$P2_12_12_1$	$P2_12_12_1$	$P2_12_12_1$	$P2_12_12_1$	$P2_12_12_1$
no. of reflections	80249	109387	264267	87576	77783	91340
no. of unique reflections	21731	21220	46602	23864	8919	6717
redundancy	3.7 (3.5)	5.2 (5.0)	5.7 (5.7)	3.7 (3.6)	8.7 (8.6)	13.6 (13.9)
completeness	94.8 (87.7)	96.8 (94.6)	100 (100)	82 (79.3)	100 (100)	100 (100)
R_{sym} (%)	5.9 (17.4)	5.6 (25.2)	7.2 (37.6)	6.7 (29.5)	14.9 (42.3)	17.0 (32.3)
I/σ	13.0 (5.9)	22.4 (3.3)	13.6 (4.4)	10.7 (4.0)	11.7 (4.8)	13.4 (7.8)
			Refinement			
no. of protein atoms	2723	2734	2693	2708	2715	2715
no. of ligand atoms	24	11	25	31	9	8
no. of water atoms	153	164	232	167	40	39
no. of reflections in refinement	19698	20096	44219	22579	7757	5619
no. of reflections in test set	1994	1083	2315	1247	1123	1063
R factor (%)	16.4	16.6	19.86	16.6	17.0	19.43
R_{free} (%)	21.7	22.2	21.81	20.4	23.9	26.18
rmsd from ideal geometry						
bonds (Å)	0.019	0.020	0.004	0.019	0.011	0.007
angles (deg)	1.9	1.9	1.2	1.9	1.5	1.26
average B factor (Å^2)	22.2	24.3	35	21.47	24.9	21.8
Ramachandran plot (%)						
most favored region	97	97.8	97.5	97.3	92.6	91.5
additional allowed region	2.5	1.93	1.92	2.2	6.27	6.81
disallowed region	0.55	0.28	0.55	0.55	1.09	1.63

[a]Values in parentheses represent the data in the highest-resolution shell.

NaOH, and finally, the pH was adjusted to 8.0. Prior to the crystallization setup, each of these ligands at 10 mM was incubated with an ∼9 mg/mL protein solution [0.5 M NaCl, 10 mM HEPES (pH 7.6), and 2 mM L-cysteine] for 1 h on ice, and later the trays were set by equilibrating 2 μL of the protein with the ligand complex against 1 μL of reservoir solution [0.225 M $MgCl_2$, 25% PEG 3350, and 0.1 M Bis-Tris (pH 5.5)]. For NE0047−cytosine complex, the reservoir solution consists of 0.225 M $MgCl_2$ and 25% PEG 3350. Thin platelike crystals were obtained in one week, and these crystals were cryoprotected with a solution containing reservoir solution combined with 5% glycerol, 5% sucrose, and 5% ethylene glycol and flash-cooled in liquid nitrogen. The X-ray diffraction data for all these complexes were collected at beamline BM-14 (European Synchrotron Radiation Facility, Grenoble, France) using a MAR CCD detector, oscillation of 1°, and an exposure time of 10 s. The crystal−detector distance varies for different complexes and was in the range of 140−250 mm. The data were processed (indexing, integration, and scaling[19]) in iMOSFLM,[20] and all crystals belonged to orthorhombic space group $P2_12_12_1$. Further refinement and structure solution were performed using CCP4i,[21] REFMAC5,[22] and CNS[23] using the native NE0047 structure (PDB entry 2G84) as the search model for molecular replacement. Model building was conducted using COOT.[24] All figures were made using PyMOL.[25] Data collection and refinement statistics are summarized in Table 1.

Ligand Binding Experiments. Calorimetry experiments were performed for NE0047 with 2′-deoxyguanosine, cytidine, and ammeline using a MicroCal iTC200 instrument (GE Healthcare). The protein samples were prepared in 50 mM HEPES and 100 mM NaCl (pH 7.5) (buffer A). Two microliters of 0.8 mM 2′-deoxyguanosine and 1.2 mM cytidine were added to a sample cell containing 22 μM full length NE0047 with the syringe at a constant stirring rate of 1000 rpm. A total of 19 injections were performed with 120 s between each successive injection. The ITC experiment with ammeline was conducted by adding 1.6 mM ammeline to 45 μM full length NE0047 at a constant stirring rate of 1000 rpm, with a duration of 30 s and with 300 s between each successive injection for a total of 19 injections. The temperature was maintained at 25 °C for all the ITC experiments. To nullify the

dx.doi.org/10.1021/bi400818e | Biochemistry 2013, 52, 8106−8114

effect of the heat of dilution, both ligands were titrated against buffer A, and the data were subtracted from the raw data prior to model fitting.

RESULTS AND DISCUSSION

Why Base Substitutions Are Not Allowed. To understand why GDs do not exhibit any deaminase activity toward guanine analogues, X-ray structures of NE0047 in complex with 9-methylguanine and 2,6-diaminopurine were determined at 2.0 Å resolution. The difference map shows clear density for the presence of both ligands in subunit A of the dimeric enzyme (Figure 2A,B). However, in subunit B, because of noise in the map, we were unable to fit the ligands. Because 9-methylguanine and 2,6-diaminopurine are nonsubstrates, it is possible that their binding initiates partial closure of the catalytically important C-terminal loop, resulting in it adopting multiple conformations thereby leading to a buildup of density that is untraceable.

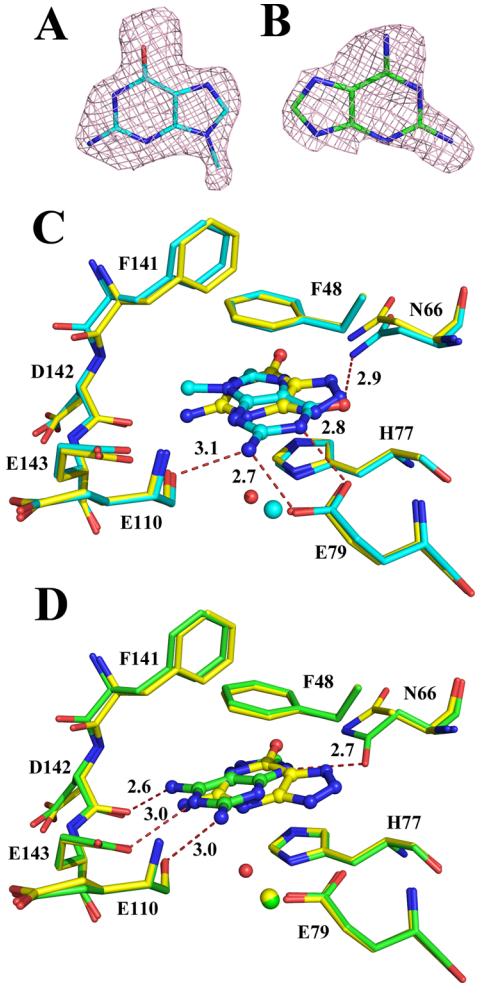

Figure 2. Active site superimposition of different complexes of NE0047. (A) Electron density ($F_o - F_c$) map contoured at 3σ for 9-methylguanine. (B) Electron density ($F_o - F_c$) map contoured at 3σ for 2,6-diaminopurine. (C) Superposition of the NE0047−9-methylguanine and NE0047−8-azaguanine complexes. (D) Superimposition of the NE0047−2,6-diaminopurine and NE0047−8-azaguanine complexes. Carbon atoms of the NE0047−8-azaguanine complex are colored yellow, those of the NE0047−9-methylguanine complex cyan, and those of the NE0047−2,6-diaminopurine complex green. All the ligands are represented as ball and stick models. The zinc atom in each superposition is shown in the respective color, and the zinc-coordinated water molecule is shown as a red sphere. Oxygen atoms are colored red and nitrogen atoms blue.

The crystal structures of NE0047 complexed with 9-methylguanine and with 8-azaguanine (PDB entry 4HRQ) were compared as shown in Figure 2C, and it was observed that no major structural changes have occurred in the amino acids forming the active site pocket. However, the orientation of 9-methylguanine has changed drastically, with the purine ring rotated by approximately 90° along the axis perpendicular to the aromatic ring system with respect to that observed for 8-azaguanine. This rotation results in the stabilization of 9-methylguanine via stacking interactions of the purine ring with residues F48 and H77 present in the binding pocket. Moreover, to preserve the interaction with the O6 atom of 9-methylguanine (2.9 Å), the side chain of N66 has shifted 0.5 Å toward the ligand (Figure S1A, Supporting Information). In addition, to ensure the proper anchoring of the ligand and to avoid steric clashes, residue F141 swings 0.6 Å in the 9-methylguanine−NE0047 complex. This movement introduces additional stabilization via favorable hydrophobic interactions between the methyl group at position 9 of the ligand and residue F141 (Figure 2C). However, this reorganization forces the amino group attached to the C2 atom to shift by 4.9 Å from the original position as observed in the 8-azaguanine−NE0047 complex. As a result, the amino group moves away from E143 and toward E79, thereby forming a hydrogen bond with the carbonyl group ($O^{\varepsilon 2}$ atom) of E79 (2.7 Å). In addition, the N1 atom of 9-methylguanine is also within hydrogen bonding distance of E79 (2.8 Å). Because the catalytically important E79 is now completely hydrogen bonded with the ligand, it is unable to abstract the proton from the catalytic water molecule. Furthermore, the increased distance of the amino group from E143 prevents the abstraction of the proton required for collapse of the tetrahedral intermediate, rendering the enzyme catalytically incompetent.

A similar scenario is observed in the case of 2,6-diaminopurine, in which the enzyme is unable to act on it. A superposition of the structures of NE0047 complexed with 2,6-diaminopurine and 8-azaguanine shows that 2,6-diaminopurine, like 9-methylguanine, has also rotated by approximately 90° with respect to the position occupied by 8-azaguanine (Figure 2D). Besides, it was observed that 2,6-diaminopurine has translated outward toward active site flap residues 140−144. This results in the amino group at position 2, which is supposed to be deaminated, moving 3.3 Å in comparison with the position of the amino group of 8-azaguanine (Figure 2D). In this orientation, the amino group is no longer within hydrogen bonding distance of E143; instead, it interacts with the backbone carbonyl oxygen atom of E110 (3.0 Å). Moreover, the second amino group at position 6 is stabilized by the formation of a hydrogen bond with the backbone carbonyl oxygen atom of D142 (2.6 Å) (Figure S1B, Supporting Information). Closer examination of the structure reveals that the rotation of the 2,6-diaminopurine is initiated to prevent the unfavorable interaction introduced by replacement of a carbonyl group with the amino group at position 6. If the ligand was to retain an orientation similar to that exhibited by 8-azaguanine, the amino group will be in the proximity of the amide nitrogen atom of N66, which is undesirable. Hence, the reshuffling of the purine ring occurs such that N66 interacts with the N9 atom of the ligand, resulting in further stabilization. Because of these changes in the orientation of the ligand, even

dx.doi.org/10.1021/bi400818e | *Biochemistry* 2013, 52, 8106−8114

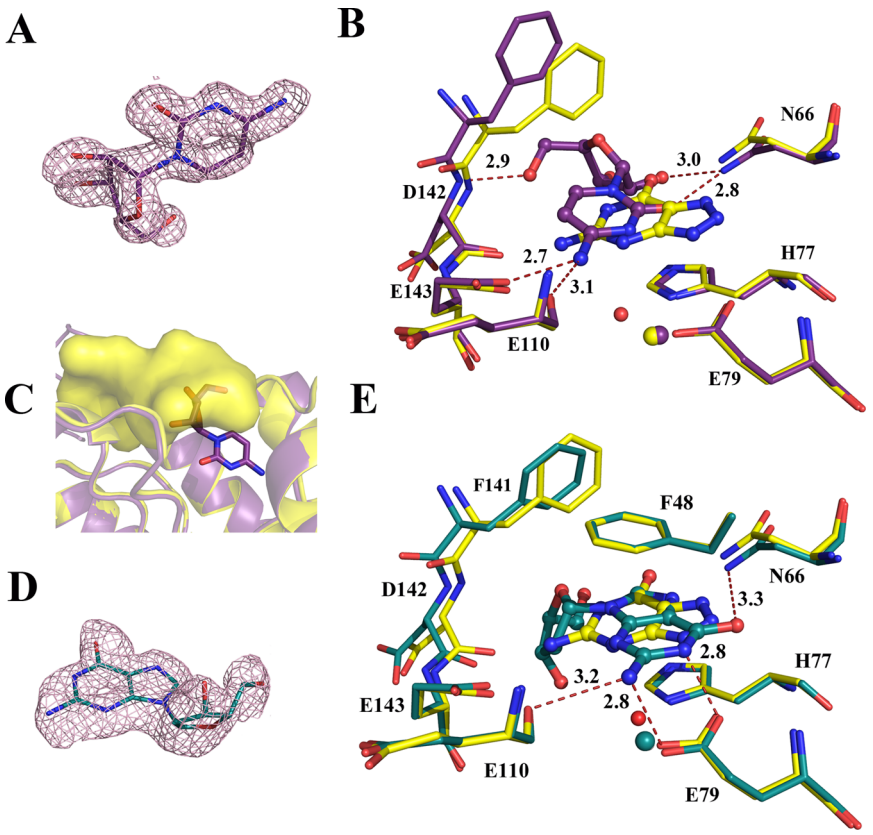

Figure 3. Active site superimposition of different complexes of NE0047. (A) Electron density ($F_o - F_c$) map contoured at 3σ for cytidine. (B) Active site superimposition of the NE0047−cytidine and NE0047−8-azaguanine complexes. (C) Model of the C-terminal loop (surface representation) on top of the active site of the structure of the NE0047−cytidine complex showing the clash of the ribose moiety with the loop. (D) Electron density ($F_o - F_c$) map contoured at 3σ for 2′-deoxyguanosine. (E) Active site superimposition of the NE0047−2′-deoxyguanosine and NE0047−8-azaguanine complexes. Carbon atoms of the NE0047−8-azaguanine complex are colored yellow, those of the NE0047−cytidine complex violet, and those of the NE0047−2′-deoxyguanosine complex dark green. All the ligands are represented as ball and stick models. The zinc atom in each superposition is shown in the respective color, and the zinc-coordinated water molecule is shown as a red sphere. Oxygen atoms are colored red and nitrogen atoms blue.

though E79 is capable of generating a hydroxide ion from the catalytic water molecule, the final release of ammonia does not take place as both the amino groups are quite far from the catalytic E143 residue. Therefore, on the basis of the information obtained from the two crystal structures described above, we conclude that any substitution in the guanine base is not tolerated, and tweaking of the structure results in the failure of the ligand to adopt the proper position in the active site, required for effective deamination.

Why GDs Do Not Catalyze Nucleosides. The fidelity of NE0047 toward its substrates is apparent because even the addition of ribose sugar moiety to its substrate guanine makes the enzyme inactive toward it. Therefore, to understand the structural basis of specificity, we have determined the crystal structures of NE0047 in complex with both purine and pyrimidine nucleosides (2′-deoxyguanosine and cytidine, respectively). The crystal structure of the cytidine−NE0047 complex reveals that like all other inhibitors, cytidine was preferentially bound only to subunit A (Figure 3A). A comparison of the active site architecture of NE0047 in complex with cytidine and 8-azaguanine is depicted in Figure 3B. Because of the presence of the bulkier ribose ring in cytidine, the active site opens up and the catalytic loop spanning residues 133−143 has slightly shifted, with the average rmsd being 0.8 Å. As a consequence, the pyrimidine ring of cytidine laterally moves by 1.1 Å toward the flap of the active site and is thereby stabilized via hydrophobic interactions with the aromatic ring system of F141 and V136. This motion also results in the amino group of cytidine rotating its position by ∼15° with respect to what is observed in the 8-azaguanine complex. The ribose sugar adopts a C2 exo conformation in this structure and is stabilized by hydrogen bonding interactions of the O5* and O2* atoms of the sugar with the backbone NH group of D142 (2.9 Å) and with the $N^{\delta 2}$ atom of N66 (3.0 Å), respectively. Additionally, to facilitate the stabilization of the O2 atom of the pyrimidine base, the active site residue N66 has shifted by 0.5 Å (Figure S1C, Supporting Information).

Nevertheless, in this orientation, the amino group of cytidine is within hydrogen bonding distance of E143 (2.7 Å) and the C4 atom (where the nucleophilic attack is expected to occur) is in the proximity of the catalytic water molecule. Hence, it seems that the amino group at position 4 is ideally situated for deamination, as both residues E79 and E143 can act as proton shuttles. Therefore, it was surprising that NE0047 exhibits no deamination activity toward cytidine. An overlay of the cytidine and 8-azaguanine bound structures shows that the major structural difference between the two complexes is in the C-terminal loop region (residues 180−189). This loop is ordered in the 8-azaguanine complex, forming a flap on top of the active site, while this loop is disordered in the cytidine complex. It has been previously demonstrated that the C-terminal loop is

dx.doi.org/10.1021/bi400818e | *Biochemistry* 2013, 52, 8106−8114

essential for function, and its effective closure induces the conformational change in the adjacent catalytic loop, thereby communicating the progress of the reaction via the dimeric interface.[16] However, if the C-terminal loop closure were to occur in the case of the cytidine complex, it would result in a steric clash with the ribose moiety, as illustrated in Figure 3C. Hence, we can conclude that binding of cytidine impedes loop closure, leading to a loss of deamination activity.

Similarly, to understand the binding mode of purine nucleosides, the crystal structure of NE0047 in complex with 2′-deoxyguanosine was determined to a resolution of 1.8 Å, and the difference density is depicted in Figure 3D. To accommodate the 2′-deoxyguanosine moiety, the catalytic helix−loop motif (residues 133−142) unique to GDs has shifted by 0.7 Å from the original position, resulting in a slight opening of the active site pocket. However, because of the presence of the bulkier nucleoside moiety, the purine ring is now pushed toward the interior of the pocket, and the space that was earlier occupied by the amino group (in the 8-azaguanine structure) is now taken up by the sugar moiety (Figure 3E). The amino group of 2′-deoxyguanosine is no longer within hydrogen bonding distance of E143 and has shifted 4.8 Å compared to that for the 8-azaguanine-bound structure. This results in the amino group making a direct hydrogen bonding interaction with E79 (2.8 Å), which further prevents residue E79 from generating the hydroxide nucleophile, thereby impeding the reaction (Figure S1D, Supporting Information). Additionally, like the case of cytidine, the larger size of the 2′-deoxyguanosine moiety also prevents the closure of the extreme C-terminal loop and inhibits catalysis (Figure S2, Supporting Information).

Evidence that nucleoside binding destroys the interdomain communication via the dimeric interface was further obtained by conducting ITC experiments on the native NE0047 protein with cytidine and 2′-deoxyguanosine moieties (Table 2 and Figure S3A,B, Supporting Information). ITC experiments show that data obtained for both ligands can be unambiguously fit to a sequential binding model, similar to that observed for 8-azaguanine. Although the binding affinity in the first site in these nucleosides is comparable to that of the substrate 8-azaguanine, the affinity for the second binding site is very weak (Table 2). This indicates that nucleosides preferentially bind to only one site and thus prevent the protein from further accepting any ligand in the second dimeric subunit. In essence, ITC results reaffirm the crystallographic finding of the recurring absence of the ligand in the second subunit. Hence, we conclude that binding of inhibitors to the active site of GDs forces the GD dimer into a catalytically compromised conformation and locks the enzyme such that the cross talk between the subunits is destroyed.

Table 2. ITC Data for the Binding of Different Ligands to NE0047

compound	K_1 (M^{-1})	K_2 (M^{-1})
8-azaguanine[16]	$(1.4 \pm 0.37) \times 10^5$	$(6.1 \pm 0.9) \times 10^3$
ammeline	$(1.2 \pm 0.13) \times 10^6$	$(1.9 \pm 0.29) \times 10^3$
cytidine	$(4.3 \pm 0.87) \times 10^4$	602 ± 235
2′-deoxyguanosine	$(9.1 \pm 0.25) \times 10^4$	853 ± 280

Why NE0047 Accepts Ammeline as a Substrate. Ammeline (4,6-diamino-2-hydroxy-1,3,5-triazine) loosely resembles pyrimidine-like cytosine; it contains an extra amino group at position 6 and a nitrogen atom at position 5 (Figure 1). Although ammeline and cytosine both are six-membered ring compounds, GDs selectively accept the former as a substrate but not the latter. To understand the structural basis of such dual specificity, the crystal structure of NE0047 with ammeline was determined at 2.7 Å resolution. Intriguingly, unlike all the other compounds, which show preferential binding of the ligand in subunit A, ammeline binds in subunit B (Figure 4A). The superimposition of NE0047 in complex with ammeline and 8-azaguanine reveals that both ligands are located in a similar orientation in the active site pocket with their interaction networks being almost analogous (Figure 4B). However, because of molecular differences in the compounds, there are subtle alterations introduced into their stabilization profile.

The crystal structure of the NE0047−ammeline complex shows that the smaller size of ammeline (in comparison with guanine) allows the N66 residue to adopt an alternate rotamer, thereby providing additional stabilization of the ligand via hydrogen bonding interactions with the O2 atom (2.5 Å) of ammeline. Moreover, the amino group at position 4 that is deaminated is stabilized by hydrogen bonding interactions of the backbone carbonyl oxygen atom of E110 (3.0 Å). In addition, this amino group is ∼3.2 Å from the E143 residue, and the carbon atom where the nucleophilic attack occurs is also in the proximity of the catalytic water molecule. This catalytic water molecule is in turn 2.7 Å from the carboxylic group of E79, thereby allowing its activation (Figure S1E, Supporting Information). Hence, the position and orientation of ammeline in the active site are extremely favorable for deamination. Further computational studies are underway to understand the mechanism of specificity toward deamination for both ligands, guanine and ammeline.

It has been established that the C-terminal loop is important for catalysis; both ITC studies and activity assay studies were performed with ammeline on full length and ΔC truncated forms of the enzymes (where the extreme nine amino acids have been removed). The results reveal that as in the case of 8-azaguanine, ammeline also binds the full length version of the enzyme, exhibiting an effective sequential binding profile (Table 2 and Figure S3C, Supporting Information). However, in the case of ammeline, the affinity in the first binding site is slightly higher in comparison with that of 8-azaguanine, which confirms the K_m value observed for NE0047 toward ammeline (1.8 mM) is higher than that toward guanine (0.7 mM).[16] Similar to guanine, the ΔC version of NE0047 also does not exhibit any deamination activity toward ammeline (Figure S4, Supporting Information).[16] Nevertheless, because the resolution of the ammeline-bound structure is ∼2.7 Å as opposed to 1.9 Å for the 8-azaguanine complex, clear density for the C-terminal loop in chain B was not observed. Hence, using the previously published coordinates (PDB entry 4HRQ), the C-terminal loop was modeled on top of the ammeline-bound structure (Figure 4C). It was observed that C-terminal loop residues A187 and R188 are in the proximity of the ammeline moiety and can form potential hydrogen bonds, thereby further stabilizing the transition state during deamination. Both 8-azaguanine and ammeline exhibit a structural correspondence in this region and are capable of interacting with the C-terminal loop via interaction of the ring nitrogen atoms (position 1 in both ligands). Therefore, it appears that ammeline is in a catalytically favorable orientation being in the proximity of both mechanistically important glutamic acids and the deamination

dx.doi.org/10.1021/bi400818e | Biochemistry 2013, 52, 8106−8114

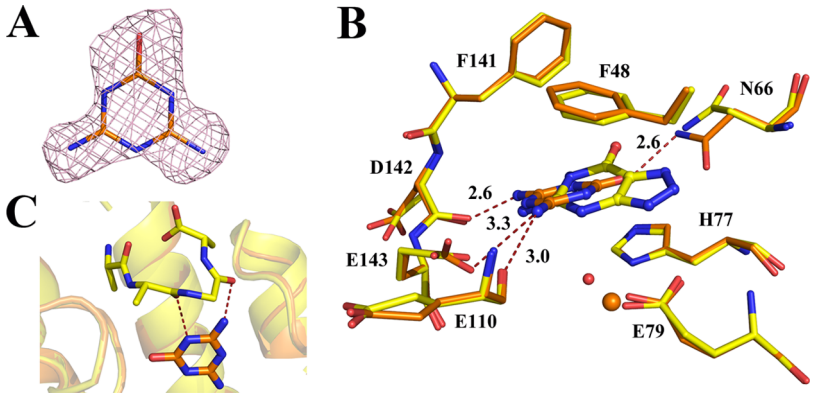

Figure 4. (A) Electron density ($F_o - F_c$) map contoured at 3σ for ammeline. (B) Active site superimposition of the NE0047−ammeline and NE0047−8-azaguanine complexes. (C) Model of the C-terminal loop on top of the active site of the structure of the NE0047−ammeline complex showing the favorable interactions of the loop with the ligand. Carbon atoms of the NE0047−8-azaguanine complex are colored yellow and those of the NE0047−ammeline complex orange. Both ligands are represented as ball and stick models. The zinc atom in each superposition is shown in the respective color, and the zinc-coordinated water molecule is shown as a red sphere. Oxygen atoms are colored red and nitrogen atoms blue.

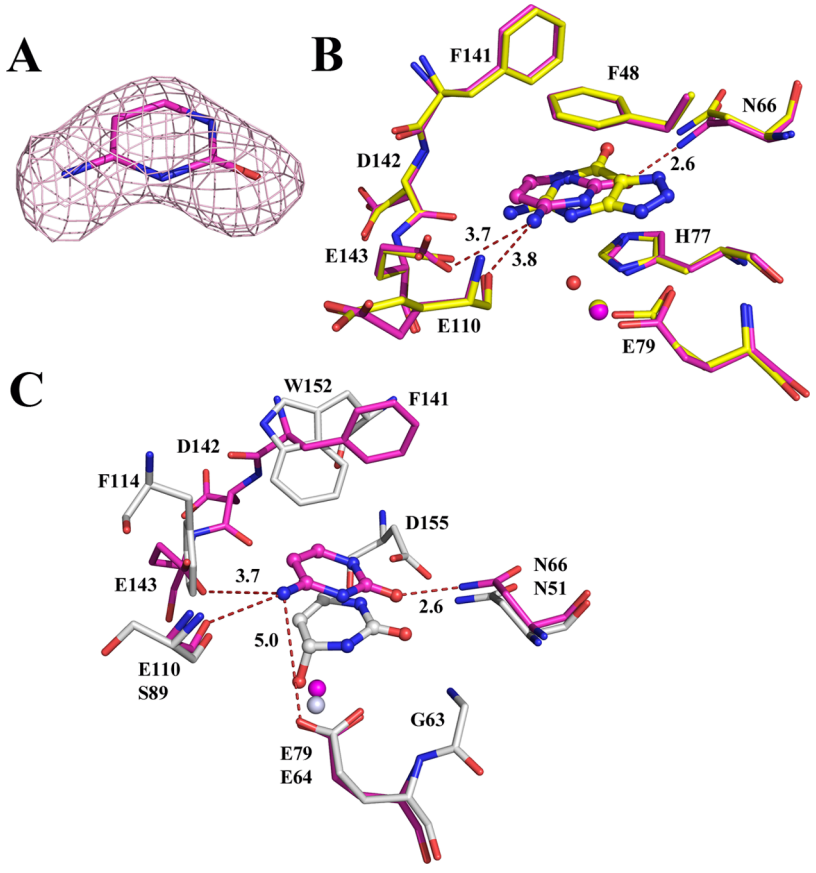

Figure 5. (A) Electron density ($F_o - F_c$) map contoured at 3σ for cytosine. (B) Active site superimposition of the NE0047−cytosine and NE0047−8-azaguanine complexes. (C) Active site superposition of cytosine-bound NE0047 and DHU-bound yeast cytosine deaminase (PDB entry 1UAQ). Carbon atoms of the NE0047−8-azaguanine complex are colored yellow, those of the NE0047−cytosine complex magenta, and those of the yCD−DHU complex gray. All the ligands are represented as ball and stick models. The zinc atom in each superposition is shown in the respective color, and the zinc-coordinated water molecule is shown as a red sphere. Oxygen atoms are colored red and nitrogen atoms blue.

is also facilitated by proper closure of the C-terminal loop, which was not possible in the case of nucleosides.

Why Cytosine Is Not Accepted as a Substrate of GD. It was evident from the crystal structure of the NE0047−cytidine complex that nucleosides with pyrimidine bases are not accepted because of improper loop closure. However, it was still not clear why even smaller pyrimidines like cytosine are not catalyzed by this enzyme. Hence, to provide insight, the crystal structure of NE0047 with cytosine bound at 3.0 Å resolution was determined, and it shows clear difference density for cytosine in the active site (Figure 5A). The cytosine molecule exhibits pseudomirror symmetry along the N3−C6 axis; a slight difference in the mass of the oxygen atom and nitrogen atom makes it difficult to distinguish them using crystallography.

dx.doi.org/10.1021/bi400818e | *Biochemistry* 2013, 52, 8106−8114

Hence, there are two potential ways to adjust cytosine in the active site. In the first plausible mode of binding, the amino group of the base points away from the E143 residue, while in the other, the amino group faces the E143 residue. Attempts were made to refine the complex structure by keeping cytosine in these two orientations; it was found that the overall placement of the cytosine ring for both positions is similar to that observed for ammeline. It is noted that in the first orientation, the deamination reaction cannot occur as the amino group is too far from both catalytically important proton shuttles, E143 and E79. However, in the second orientation, the binding of cytosine is mainly stabilized by hydrogen bonding interactions between its keto group and N66 (2.6 Å) (Figure 5B), and in this mode, it is not effectively stabilized. Nevertheless, assuming that cytosine adopts this orientation, one of the prime reasons for the absence of activity is the increased distance between the cytosine amino group and E143 (3.6 Å), which may be enough to impede shuttling of the proton.

To improve our understanding of why GDs do not catalyze cytosine, we compared the structure of the NE0047−cytosine complex with the structure of yeast cytosine deaminase (yCD) complexed with cytosine inhibitor 3,4-dihydrouracil (DHU)[15] (Figure 5C). Because cytosine is the primary substrate for yCD, structural differences observed for cytosine bound to NE0047 versus DHU bound to yCD provide clues about the evolutionary divergence adopted by the CDA family of enzymes to achieve a high degree of substrate specificity. It was observed that in yCD, the DHU directly coordinates to the catalytic zinc atom and also interacts with the catalytic E64 (2.5 Å), thus facilitating zinc-assisted deamination. However, in the structure of NE0047 complexed with cytosine, the amino group is 5.0 Å from the corresponding catalytic E79 residue and 4.6 Å from the zinc atom (Figure S1F, Supporting Information). Thus, cytosine in GD has translated by ∼2.0 Å from the position of DHU in yCD, away from the metal ion (Figure 5C). In addition, a superposition of the structure of NE0047 with yCD showed that no residue analogous to E143 in NE0047 was observed in yCD. This demonstrates that for the deamination of cytosine, only one negatively charged residue (E64 in yCD, equivalent to E79 in NE0047) is sufficient,[15,26] and unlike guanine deamination, it does not require presence of two negatively charged residues.[16]

A comparison of the ligand binding pocket of yCD with that of NE0047 reveals considerable divergence in the secondary structure elements of the ligand binding pocket between the two proteins, and the cytosine is also anchored in the two structures via a dissimilar hydrogen bonding scheme. The key catalytic loop−helix region lining the active site present in NE0047 and other GDs is missing in yCD and is instead replaced by a C-terminal helix that is responsible for compaction of the ligand binding pocket, and in addition, this contains a conserved aspartate residue (D155). D155 in yCD has been reported to play an important role in conferring substrate specificity.[15] Thus, the comparison described above leads us to the conclusion that CDs are evolutionarily distinct from GDs and achieve substrate specificity by employing a slightly altered mechanism and by making their active site more compact.

CONCLUSION

In this work, the structural basis of ligand specificity of NE0047, a CDA superfamily GD, was investigated in depth. By solving and analyzing a series of X-ray structures with nucleobases and their nucleoside analogues in complex with NE0047, we established that the active site is engineered to select out any substitutions in the base scaffold. Additionally, it was also found that nucleosides preferentially bind to only one of the two active sites, thereby locking the enzyme in a conformation that is incapacitated with respect to enzyme turnover. The closure of the catalytically crucial C-terminal loop is also severely hampered by the sugar moiety of the nucleoside, further abrogating deamination. Moreover, by using structural and biochemical tools, we unravelled why NE0047 accepts ammeline (a triazine, intermediate in the melamine pathway) as a secondary substrate. It was found that unlike other compounds, ammeline not only binds in the active site in a catalytically favorable conformation in the proximity of the two proton shuttles but also favors proper anchoring of the C-terminal flap for efficient catalysis. On the other hand, it was observed that cytosine is unable to position itself into the NE0047 active site in a favorable conformation, which facilitates deamination. Therefore, on the basis of the active site correspondence of other GDs with NE0047 that belong to the CDA superfamily, these results can be extended to provide insights into the structural basis of ligand specificity in this class of enzymes.

ASSOCIATED CONTENT

Supporting Information

Figures S1−S4. This material is available free of charge via the Internet at http://pubs.acs.org.

AUTHOR INFORMATION

Corresponding Author

*Department of Chemistry, IIT Bombay, Powai, Mumbai 400076, India. E-mail: ruchi@chem.iitb.ac.in. Phone: 91-22-2576 7165.

Funding

This work was supported by IIT Bombay, DBT (BT/PRI3766/BRB/10/785/2010), and DST (SR/S/BB-53/2010).

Notes

The authors declare no competing financial interest.

ACKNOWLEDGMENTS

We thank the Midwest center for structural genomics consortium for providing the NE0047 plasmid. We thank the DBT-India consortium and BM-14 of the European Synchrotron Radiation Facility, the National Institute of Immunology, Delhi, for providing a facility for X-ray data collection, and IIT Bombay for providing the necessary infrastructure. We also thank Prof. V. K. Singh and other colleagues at IIT Bombay for helpful discussions.

ABBREVIATIONS

GD, guanine deaminase; CDA, cytidine deaminase; bGD, *B. subtilis* guanine deaminase; AHS, amidohydrolase superfamily; DHU, 3,4-dihydrouracil; yCD, yeast cytosine deaminase; ITC, isothermal titration calorimetry; TIM, triosephosphate isomerase; PDB, Protein Data Bank; ΔC, NE0047 (residues 1−180); HEPES, 2-[4-(2-hydroxyethyl)piperazin-1-yl]ethanesulfonic acid; rmsd, root-mean-square deviation.

REFERENCES

(1) Maynes, J. T., Yuan, R. G., and Snyder, F. F. (2000) Identification, expression, and characterization of *Escherichia coli* guanine deaminase. *J. Bacteriol. 182*, 4658−4660.

(2) Liaw, S. H., Chang, Y. J., Lai, C. T., Chang, H. C., and Chang, G. G. (2004) Crystal Structure of *Bacillus subtilis* Guanine Deaminase. *J. Biol. Chem. 279*, 35479−35485.

(3) Yuan, G., Bin, J. C., McKay, D. J., and Snyder, F. F. (1999) Cloning and characterization of human guanine deaminase. Purification and partial amino acid sequence of the mouse protein. *J. Biol. Chem. 274*, 8175−8180.

(4) Paletzki, R. F. (2002) Cloning and characterization of guanine deaminase from mouse and rat brain. *Neuroscience 109*, 15−26.

(5) Nygaard, P., Bested, S. M., Andersen, K. A., and Saxild, H. H. (2000) *Bacillus subtilis* guanine deaminase is encoded by the yknA gene and is induced during growth with purines as the nitrogen source. *Microbiology 146*, 3061−3069.

(6) Fernández, J. R., Byrne, B., and Firestein, B. L. (2009) Phylogenetic analysis and molecular evolution of guanine deaminases: From guanine to dendrites. *J. Mol. Evol. 68*, 227−235.

(7) Cook, A. M., Grossenbacher, H., and Hutter, R. (1984) Bacterial degradation of N-cyclopropylmelamine. The steps to ring cleavage. *Biochem. J. 222*, 315−320.

(8) Seffernick, J. L., Dodge, A. G., Sadowsky, M. J., Bumpus, J. A., and Wackett, L. P. (2010) Bacterial Ammeline Metabolism via Guanine Deaminase. *J. Bacteriol. 192*, 1106−1112.

(9) Ingelfinger, J. R. (2008) Melamine and the Global Implications of Food Contamination. *N. Engl. J. Med. 359*, 2745−2748.

(10) Brown, C. A., Jeong, K. S., Poppenga, R. H., Puschner, B., Miller, D. M., Ellis, A. E., Kang, K.-I., Sum, S., Cistola, A. M., and Brown, S. A. (2007) Outbreaks of Renal Failure Associated with Melamine and Cyanuric Acid in Dogs and Cats in 2004 and 2007. *Journal of Veterinary Diagnostic Investigation 19*, 525−531.

(11) Holm, L., and Sander, C. (1997) An evolutionary treasure: Unification of a broad set of amidohydrolases related to urease. *Proteins 28*, 72−82.

(12) Lai, W. L., Chou, L. Y., Ting, C. Y., Kirby, R., Tsai, Y. C., Wang, A. H. J., and Liaw, S. H. (2004) The Functional Role of the Binuclear Metal Center in D-Aminoacylase. *J. Biol. Chem. 279*, 13962−13967.

(13) Fernández, J. R., Welsh, W. J., and Firestein, B. L. (2008) Structural characterization of the zinc binding domain in cytosolic PSD-95 interactor (cypin): Role of zinc binding in guanine deamination and dendrite branching. *Proteins 70*, 873−881.

(14) Betts, L., Xiang, S., Short, S. A., Wolfenden, R., and Carter, C. W., Jr. (1994) Cytidine deaminase. The 2.3 Å crystal structure of an enzyme:transition-state analog complex. *J. Mol. Biol. 235*, 635−656.

(15) Ko, T. P., Lin, J. J., Hu, C. Y., Hsu, Y. H., Wang, A. H., and Liaw, S. H. (2003) Crystal structure of yeast cytosine deaminase. Insights into enzyme mechanism and evolution. *J. Biol. Chem. 278*, 19111−19117.

(16) Bitra, A., Hussain, B., Tanwar, A. S., and Anand, R. (2013) Identification of Function and Mechanistic Insights of Guanine Deaminase from *Nitrosomonas europaea*: Role of the C-Terminal Loop in Catalysis. *Biochemistry 52*, 3512−3522.

(17) Yao, L., Cukier, R. I., and Yan, H. (2007) Catalytic Mechanism of Guanine Deaminase: An ONIOM and Molecular Dynamics Study. *J. Phys. Chem. B 111*, 4200−4210.

(18) Caraway, W. T. (1966) Colorimetric Determination of Serum Guanase Activity. *Clin. Chem. 12*, 187−193.

(19) Evans, P. (2006) Scaling and assessment of data quality. *Acta Crystallogr. D62*, 72−82.

(20) Battye, T. G. G., Kontogiannis, L., Johnson, O., Powell, H. R., and Leslie, A. G. W. (2011) iMOSFLM: A new graphical interface for diffraction-image processing with MOSFLM. *Acta Crystallogr. D67*, 271−281.

(21) Project, C. C. (1994) The CCP4 Suite: Programs for Protein Crystallography. *Acta Crystallogr. D4*, 760−763.

(22) Murshudov, G. N., Skubak, P., Lebedev, A. A., Pannu, N. S., Steiner, R. A., Nicholls, R. A., Winn, M. D., Long, F., and Vagin, A. A. (2011) REFMAC5 for the refinement of macromolecular crystal structures. *Acta Crystallogr. D67*, 355−367.

(23) Brunger, A. T., Adams, P. D., Clore, G. M., DeLano, W. L., Gros, P., Grosse-Kunstleve, R. W., Jiang, J. S., Kuszewski, J., Nilges, M., Pannu, N. S., Read, R. J., Rice, L. M., Simonson, T., and Warren, G. L. (1998) Crystallography & NMR system: A new software suite for macromolecular structure determination. *Acta Crystallogr. D54*, 905−921.

(24) Emsley, P., Lohkamp, B., Scott, W. G., and Cowtan, K. (2010) Features and development of Coot. *Acta Crystallogr. D66*, 486−501.

(25) DeLano, W. L. (2002) *The PyMol User's Manual*, DeLano Scientific, San Carlos, CA.

(26) Sklenak, S., Yao, L., Cukier, R. I., and Yan, H. (2004) Catalytic Mechanism of Yeast Cytosine Deaminase: An ONIOM Computational Study. *J. Am. Chem. Soc. 126*, 14879−14889.